# Electronic Structure and Spatial Arrangement of C<sub>2v</sub>-Coordinated Ferric Iron in Metmyoglobin, Metmyoglobin Fluoride, and Methemoglobin

Hermann Eicher

Physik Department der Technischen Universität München

(Z. Naturforsch. 30 c, 701-710 [1975]; received July 7, 1975)

Electronic Structure, Metmyoglobin, Metmyoglobin Fluoride, Methemoglobin

The electronic term scheme of ferric iron in metmyoglobin, metmyoglobin fluoride, and methemoglobin is evaluated by a Hamiltonian which involves the Coulomb repulsion of the 3d electrons, their interaction with the  $C_{2\nu}$ -coordinated ligands, and spin-orbit coupling. The adjustable parameters of the theory were determined by a least squares fit to experimental EPR, susceptibility, and far-infrared data reported in the literature. According to these results, the structural properties of the ferric ion and its neighboring ligands were discussed by means of group theoretical arguments: An increasing out of plane position of the ferric ion is found in the sequence metHb—metMb—MbF which corresponds to an increasing binding strength with the axial ligands.

#### I. Introduction

A great deal of experimental work has been done during the past years to determine the electronic structure of the ferric ion in biological substances. At the present state of our understanding, three methods proved to yield most valuable information regarding the low-lying energy levels within the 3d5 configuration of the ferric ion - the electron paramagnetic resonance (EPR), the measurement of static paramagnetic susceptibilities, and the techniques of far-infrared Fourier transform spectroscopy. However, the common interpretation of the experimental results in terms of the spin Hamiltonian formalism gives no insight in the detailed structure of the ferric system. This formalism acts only as a tabulation scheme in order to catalog the experimental results with fortuitous accuracy, depending on the number of adjustable parameters. In attempting to improve on this prescriptive approach, Harris et al. 1-4 evaluated within the basis set of three total five-electron multiplets  ${}^{6}A_{1}(t_{2}^{3}e^{2})$ ,  ${}^{4}\text{T}_{1}(\text{t}_{2}^{4}\text{ e})$  and  ${}^{2}\text{T}_{2}(\text{t}_{2}^{5})$  the eigenvalues and eigenvectors of the low-lying Kramers doublets of the ferric ion by means of a Hamiltonian which takes into account the Coulomb repulsion between the five 3d-electrons, the interaction with the C<sub>4v</sub>-coordinated ligands, and spin-orbit coupling. This calcu-

Requests for reprints should be sent to Dr. H. Eicher, Physik Department, Technische Universität München, D-8046 Garching bei München.

lation is a function of certain parameters which were varied until the best fit with experimental data was obtained. It should be noticed, however, that this basis set is only a suitable starting point in the limit of a strong octahedral ligand field, where contributions of the lower C4v-symmetry to the Hamiltonian are sufficiently small. From the well known structural properties of the porphyrin compounds it is obvious that at least the sixth coordination of the ferric ion is occupied by a ligand with deviating binding strength. For that reason, the adjusted parameters of the strong octahedral field approximation are related with limited accuracy to the corresponding physical interactions of the ferric system. On the other hand, the low-lying energy levels of the 3d6 configuration in Fe2+-porphyrin compounds were calculated within a basis set reflecting exactly the C<sub>4v</sub> point symmetry of the ferrous ion <sup>5</sup>. A small rhombic perturbation and spin-orbit coupling were handled as perturbations and the inherent parameters of the theory were successfully adjusted to the temperature dependent quadrupole splittings and susceptibility measurements by a least squares fit procedure 6-9. Thus, the aim of the present paper is to carry over this concept to the 3d<sup>5</sup> configuration of C<sub>2v</sub>-coordinated Fe<sup>3+</sup> in biological systems, so that the experimental results on ferrous and ferric porphyrin compounds can be discussed simultaneously. In Sec. II the formalism of the theory will be applied to the 3d5 configuration of C<sub>2v</sub>-coordinated ferric iron and the results obtained are put into a form more suitable for numerical computations. Sec. III includes a discussion of the electronic structure and the spatial arrangement of the ferric ion in metmyoglobin (Mb), metmyoglobin fluroride (MbF), and methemoglobin (Hb). The adjustable parameters of the theory are obtained by a least squares fit to temperature dependent magnetic susceptibility data <sup>10</sup>, far-infrared data <sup>11</sup>, and frequency dependent EPR data, where the anisotropy of the g-tensor in the hem plane is observed with high accuracy <sup>12, 13</sup>.

### II. Theory

The basis set of the  $3d^5$  configuration is given by the following total five-electron multiplets  ${}_{(2S+1)}L$ , where (2S+1) is the spin multiplicity, L the angular quantum number, and v the seniority number  ${}^{14, 15}$ 

$$S = 5/2: {}^{6}_{5}S;$$

$$S = 3/2: {}^{4}_{3}P, {}^{4}_{5}D, {}^{4}_{3}F, {}^{4}_{5}G;$$

$$S = 1/2: {}^{2}_{5}S, {}^{2}_{3}P, {}^{2}_{1}D, {}^{2}_{3}D, {}^{2}_{5}D, {}^{2}_{3}F, {}^{2}_{5}F, {}^{2}_{3}G, {}^{2}_{5}G, {}^{2}_{3}H, {}^{4}_{5}I.$$
(1)

In a first step we diagonalize this basis set by means of a Hamiltonian which takes into account the approximate  $C_{4\nu}$  point symmetry of the iron cation and the Coulomb repulsion between the 3d electrons. The first part of the Hamiltonian

$$\hat{\mathbf{H}}_{1} = (2/7)^{1/2} (\varepsilon_{3} - \varepsilon_{2} - \varepsilon_{1}) \hat{\mathbf{V}}_{0}^{(2)} 
+ (1/70)^{1/2} (\varepsilon_{3} + 6 \varepsilon_{2} - 8 \varepsilon_{1}) \hat{\mathbf{V}}_{0}^{(4)} 
+ 1/2 \varepsilon_{3} (\hat{\mathbf{V}}_{4}^{(4)} + \hat{\mathbf{V}}_{-4}^{(4)}),$$
(2)

is determined by the energy gaps  $\varepsilon_{\mu}$  of the anti-bonding single 3d electron orbitals

$$\begin{split} \varepsilon_{1} &= E\left(3 \operatorname{d}_{xz,yz}\right) - E\left(3 \operatorname{d}_{xy}\right), \\ \varepsilon_{2} &= E\left(3 \operatorname{d}_{z^{2}}\right) - E\left(3 \operatorname{d}_{xy}\right), \\ \varepsilon_{3} &= E\left(3 \operatorname{d}_{x^{2}-y^{2}}\right) - E\left(3 \operatorname{d}_{xy}\right). \end{split} \tag{3}$$

The second part is given by

$$\hat{\mathbf{H}}_2 = \hat{\mathbf{e}}_1 \, E_1 + \hat{\mathbf{e}}_2 \, E_2 \,, \tag{4}$$

where the coefficients  $E_1$  and  $E_2$  are certain linear combinations of the Slater integrals  $^5$  (we refer to this paper for definitions, notation, and discussions). As in the case of the ferrous system, we choose these coefficients to be  $E_1=4918~{\rm cm}^{-1}$  and  $E_2=403~{\rm cm}^{-1}$ ; deviations from the exact values yield only a renormalization of the energy scale. The matrix elements of the tensor operator  $\hat{V}_q^{(\rm K)}$  are defined by the equation

$$\langle d^{5} v, S M_{s}, L M_{L} | \hat{V}_{q}^{(K)} | d^{5} v', S' M'_{s}, L' M'_{L} \rangle$$

$$= (-1)^{L-M_{L}} \begin{pmatrix} L & K & L' \\ -M_{L} & q & M'_{L} \end{pmatrix}$$

$$\langle d^{5} v S L || \hat{V}^{(K)} || d^{5} v' S L' \rangle \delta(S S') \delta(M_{s} M'_{s}).$$

$$(5)$$

The reduced matrix elements of the second rank tensor  $\hat{V}^{(2)}$  are proportional to those calculated by Racah <sup>14</sup>

$$\langle d^5 v \, S \, L \, \| \, \hat{\mathbf{V}}^{(2)} \, \| \, d^5 v' \, S \, L' \rangle = (5^{1/2}/35) \, \langle d^5 v \, S \, L \, \| \, 35 \, \hat{\mathbf{U}}^{(2)} \, \| \, d^5 v' \, S \, L' \rangle , \quad (6)$$

and the reduced matrix elements of the tensor operator  $\hat{V}^{(4)}$  are listed in Table I. The required matrix elements of the two-particle operators  $\hat{e}_1$  and  $\hat{e}_2$  in Eqn (4) are tabulated in Table II, showing that Coulomb interaction between the five 3d electrons only violates the seniority of the base vectors  ${}^2_1D$  and  ${}^2_5D$ . The secular problem within the 3d<sup>5</sup> configuration has been worked out via computer for the Hamiltonian  $\hat{H}_1 + \hat{H}_2$ , depending on the three energy gaps  $\varepsilon_\mu$ ; reasonable values of these parameters for  $C_{2v}$ -coordinated Fe<sup>3+</sup> in porphyrins and related compounds are given by

$$22000 \text{ cm}^{-1} \approx \varepsilon_3 < 28000 \text{ cm}^{-1}, 0.4 \varepsilon_3 < \varepsilon_2 < 0.8 \varepsilon_3, -200 \text{ cm}^{-1} < \varepsilon_1 < 800 \text{ cm}^{-1}.$$
 (7)

Figure 1 shows the positions of the low-lying energy levels  $^6A_1$ ,  $^4A_2$ ,  $^4E$ ,  $^2B_2$ , and  $^2E$ . In order to under-

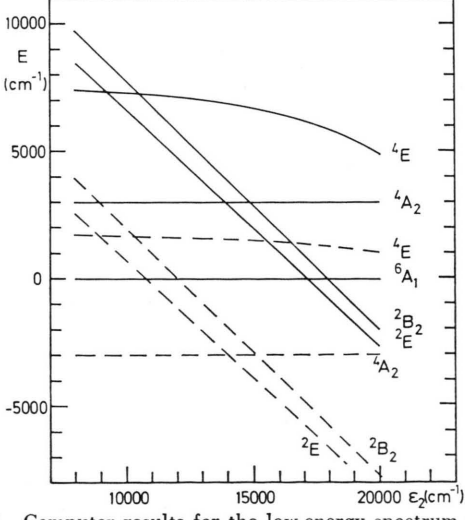


Fig. 1. Computer results for the low-energy spectrum within the  $3d^5$  configuration of  $C_{4v}$ -coordinated Fe³+, plotted as a function of the energy gap  $\varepsilon_2$ . The solid and the dashed lines represent two different calculations using the parameters  $\varepsilon_1 = 600 \text{ cm}^{-1}$ ,  $\varepsilon_3 = 22000 \text{ cm}^{-1}$ , and  $\varepsilon_1 = 600 \text{ cm}^{-1}$ ,  $\varepsilon_3 = 28000 \text{ cm}^{-1}$ , respectively.

S = 5/2:	$\langle d^{5}, {}^{6}_{5}\mathrm{S} \parallel \widehat{\mathrm{V}}^{\scriptscriptstyle{(4)}} \parallel d$	$d^{5}, {}^{6}_{5}S\rangle = 0$ .		
S=3/2:	<b>⁴</b> P	5D	<b>⁴</b> F	åG
<sup>4</sup> <sub>3</sub> P <sup>4</sup> <sub>5</sub> D	0	0	$0 \\ -3 (10/7)^{1/2}$	3 (2) 1/2
<sup>3</sup> F ⁴G	$-3(2)^{1/2}$	$3(10/7)^{1/2}$	$0 \\ -3(11/7)^{1/2}$	$3(11/7)^{1/2}$

Table I. The reduced matrix elements  $\langle d^5 \, v \, S \, L \parallel V^{(4)} \parallel d^5 \, v' \, S \, L' \rangle$  between the different terms  $^{(2s+1)}{}_v \, L$  of the configuration  $3d^5$ .

S=1/2	<sup>2</sup> <sub>5</sub> S	<sup>2</sup> 3 P	<sup>2</sup> D	$^2_3\mathrm{D}$	<sup>2</sup> D
S	0	0	0	0	0
P	0	0	0	0	0
D	0	0	0	$(-5/7)(7)^{1/2}$	0
D	0	0	$(-5/7) (7)^{1/2}$	0	$(10/7) (2)^{1/2}$
D	0	0	0	$(10/7) (2)^{1/2}$	0
F	0	0	$(10)^{1/2}$	0	$(35/4)^{1/2}$
F	0	$(9/14) (7)^{1/2}$	0	$(11/14) (14)^{1/2}$	0
G	$2(6/7)^{1/2}$	0	$3(22/21)^{1/2}$	0	$(-3/14) (11/3)^{1/2}$
G	0	$-3(11/28)^{1/2}$	Ó	$(9/7) (5/2)^{1/2}$	0
H	0	0	$-(22)^{1/2}$	0	$-2(11/7)^{1/2}$
I	0	0	0	$2(13/7)^{1/2}$	0

stand the relation between the particular low energy spectrum and the parameters  $\varepsilon_{\mu}$ , we computed a variety of spectra which are not shown in this paper. From those we deduced the following empirical formulas

$$\begin{split} &E(^{6}\mathrm{A}_{1}) = 0\;, \\ &E(^{4}\mathrm{A}_{2}) = 24765 - 0.99\; \varepsilon_{3}\;, \\ &E(^{2}\mathrm{E}) = 36960 + 0.96\; \varepsilon_{1} - 0.93\; \varepsilon_{2} - 0.98\; \varepsilon_{3}\;, \\ &E(^{2}\mathrm{B}_{2}) = 37570 + 1.90\; \varepsilon_{1} - 0.98\; \varepsilon_{2} - 0.96\; \varepsilon_{3}\;, \\ &E(^{4}\mathrm{E}) = 26480 + 0.96\; \varepsilon_{1} - 0.12\; \varepsilon_{2} - 0.85\; \varepsilon_{3}\;, \end{split} \tag{8}$$

where the energies are given in units of cm<sup>-1</sup>. The eigenvalues and eigenvectors of the  ${}^4A_2$  level depend solely upon  $\varepsilon_3$ . According to Eqns (7) and (8), the  ${}^4E$  level lies at least  $3400 \, \mathrm{cm}^{-1}$  above the particular ground state, so that this term contributes only slightly to our further computations.

In the second step of the calculation, the eigenvalues and eigenvectors of the low-lying levels  $^6A_1$ ,  $^4A_2$ ,  $^2E$ ,  $^2B_2$ , and  $^4E$ , still dependent on the adjustable parameters  $\varepsilon_\mu$ , are used as base vectors

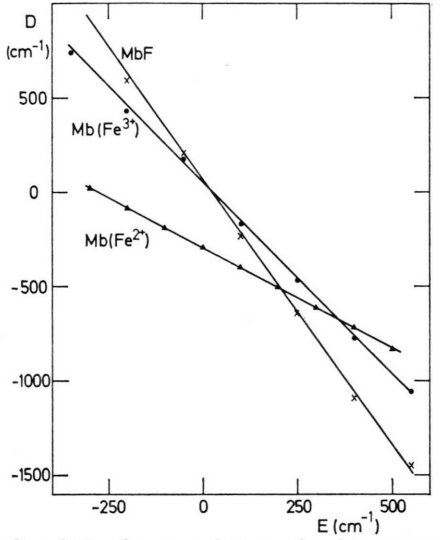


Fig. 2. Correlation between the two rhombic parameters D and E forMbF, metMb, and Mb(Fe<sup>2+</sup>) obtained by a least squares fit to the experimental data. In the case of Mb(Fe<sup>2+</sup>), the experimental data include temperature dependent susceptibility, field dependent magnetization, and Mössbauer measurements  $^9$ .

Table II. Matrix elements of the two-particle operators  $\hat{e}_1$  and  $\hat{e}_2$  for the multiplets of the configuration  $3d^5$ .

Diagonal matrix elements

	,	6 S	4 P	4 D	<sup>4</sup> <sub>3</sub> F	4 G	<sup>2</sup> <sub>5</sub> S	<sup>2</sup> <sub>3</sub> P	<sup>2</sup> 1D	<sup>2</sup> <sub>3</sub> D	<sup>2</sup> D	<sup>2</sup> <sub>3</sub> F	<sup>2</sup> F	<sup>2</sup> <sub>3</sub> G	2 G	<sup>2</sup> H	<sup>2</sup> I
ê <sub>1</sub> ê <sub>2</sub>		0	7 21	5 9	7 9	5 -5	8 24	10 60	14 0	10 12	8 18	10 -30	8 12	10 26	8	$^{10}_{-24}$	-18

Nondiagonal matrix element  $\langle 3d^5, {}_{1}^{2}D \mid \hat{e}_{2} \mid 3d^5, {}_{5}^{2}D \rangle = -12 (14)^{1/2}.$ 

for the diagonalization of the relatively weak spin-orbit interaction  $\hat{H}_3$  and rhombic perturbation  $\hat{H}_4$ . The relevant matrix elements for spin-orbit interaction

$$\hat{\mathbf{H}}_{3} = \xi \sum_{i,q} (-1)^{q} (\hat{\mathbf{s}}_{q}^{(1)} \hat{\mathbf{l}}_{-q}^{(1)})_{i}$$
 (9)

in analogy to our previous papers <sup>5, 6, 8, 9</sup>, so that the matrix element with the ferrous high-spin state <sup>5</sup>E is simply given by

$$\langle 3d^6, {}^5E_+ | \hat{H}_4 | 3d^6, {}^5E_- \rangle = D + E.$$
 (12 a)

Thus, rhombic perturbation splits the single

2 F	<sup>2</sup> <sub>5</sub> F	<sup>2</sup> G	<sup>2</sup> <sub>5</sub> G	$^2_3\mathrm{H}$	<sup>2</sup> <sub>5</sub> I
0	0	2 (6/7) 1/2	0	0	0
0 1/2	$(9/14) (7)^{1/2}$	$0 \ 3 (22/21)^{1/2}$	$3(11/28)^{1/2}$	$(22)^{1/2}$	0
$-(10)^{1/2}$	$(-11/14)(14)^{1/2}$	0	$(9/7) (5/2)^{1/2}$	0	$2(13/7)^{1/2}$
$(-1/2)(35)^{1/2}$	0	$(-3/14) (11/3)^{1/2}$	0	$2(11/7)^{1/2}$	0
0	$-(11/4)^{1/2}$	(2/2) (22/7) 1/2	$(3/2) (7)^{1/2}$	(7.42/20) 1/2	$(-7/2)(13/7)^{1/2}$
$-(11/4)^{1/2}$	$(-3/2)(33/7)^{1/2}$	$(3/2) (33/7)^{1/2}$	$(-9/14) (39)^{1/2}$	$-(143/28)^{1/2}$	$-(39/28)^{1/2}$
$(-3/2)(7)^{1/2}$	0	$(-9/14) (39)^{1/2}$	0	$-3(13/28)^{1/2}$	0
0	$-(143/28)^{1/2}$	0	$3(13/28)^{1/2}$	0	$-2(13)^{1/2}$
$(7/2) (13/7)^{1/2}$	0	$-(39/28)^{1/2}$	0	$2(13)^{1/2}$	0

are given by

$$\langle d^{5} v S M_{s} L M_{L} | \sum_{i} (\hat{s}_{q}^{(1)} \hat{l}_{-q}^{(1)})_{i} | d^{5} v' S' M_{S}' L' M_{L}' \rangle$$

$$= (-1)^{S-M_{S}} \begin{pmatrix} S & 1 & S' \\ -M_{S} & q & M_{S}' \end{pmatrix} (-1)^{L-M_{L}} \begin{pmatrix} L & 1 & L' \\ -M_{L} - q & M_{L}' \end{pmatrix}$$

$$\langle d^{5} v S L | | \sum_{i} (\hat{s}^{(1)} \hat{l}^{(1)})_{i} | | d^{5} v' S' L' \rangle, \qquad (10)$$

where the reduced matrix elements are equal to those given by Racah <sup>14</sup>

$$\langle d^5 v \, S \, L \, \| \, \sum_{i} (\hat{s}^{(1)} \, \hat{l}^{(1)})_{i} \, \| \, d^5 v' \, S' \, L' \rangle$$

$$= \langle d^5 v \, S \, L \, \| \, (30)^{1/2} \, \hat{V}^{(11)} \, \| \, d^5 v' \, S' \, L' \rangle \,. \quad (11)$$

The coupling constant  $\xi$  is a fit parameter, too. As in the case of the ferrous ion <sup>8</sup>, a reduction of the free ion value  $\xi_0 = 420 \,\mathrm{cm}^{-1}$  by approximately a factor of 0.7 is expected in the ferric porphyrin compounds.

The analysis <sup>8</sup> of the single crystal experiment on Mb (Fe<sup>2+</sup>) <sup>16</sup> yielded that the principal axes x and y of the electric field gradient (efg) tensor are oriented along the NVL 416 – NPR 418 and NVR 415 – NPL 417 directions of the pyrrole nitrogens, respectively, indicating that rhombic perturbation lowers the  $C_{4v}$  point symmetry of the iron cation to  $C_{2v}$ . In this case, the Hamiltonian  $\hat{H}_4$  is given by <sup>9, \*</sup>

$$\hat{\mathbf{H}}_{4} = (7/3)^{1/2} D(\hat{\mathbf{V}}_{2}^{(2)} + \hat{\mathbf{V}}_{-2}^{(2)}) 
- (7/4)^{1/2} E(\hat{\mathbf{V}}_{2}^{(4)} + \hat{\mathbf{V}}_{-2}^{(4)}), \quad (12)$$

where the relevant matrix elements are defined in Eqn (5). The coefficients of Eqn (12) are chosen

electron doublet  $(3d_{xz,yz})$  by an amount of 2(D+E), because, within the 3d<sup>6</sup> configuration, the single electron orbitals and their associated high-spin levels are identical. In principle, the two parameters D and E can be determined from the rhombic splittings of the orbital degenerate base vectors <sup>2</sup>E and <sup>4</sup>E. However, the low-lying Kramers doublets which will be correlated to EPR, far-infrared, and susceptibility data, are insensitive to the rhombic splitting of the high-lying 4E term. For that reason we can only fix a certain linear combination of D and E from those experiments. On the other hand, the analysis of experimental data in Sec. III indicates that the rhombic parameters are similar for ferric and ferrous hem compounds; this assumption allows to fix the two parameters

<sup>\*</sup> Note that the principal axes x and y of the efg and of the g-tensor are always parallel to the hem plane for rhombic symmetry. However, in the general case of  $C_2$ -symmetry, when the principal axes do not point towards the pyrole nitrogen positions, one must add two further terms to  $\hat{H}_4:i(7/3)^{1/2}\,D'(\hat{V}_2^{(2)}-\hat{V}_{-2}^{(2)})-i(7/4)^{1/2}\,E'(\hat{V}_1^{(4)}-\hat{V}_{-2}^{(2)})$ , which give rise to complex matrix elements. In the remainder of the paper we neglect these additional terms assuming  $C_{2\mathbf{v}}$  point symmetry of the ferrous and ferric cation in hem compounds.

separately. As mentioned above, the required matrix elements of  $\hat{H}_3 + \hat{H}_4$  with the base-vectors depend implicitly upon the parameters  $\varepsilon_1$ ,  $\varepsilon_2$ , and  $\varepsilon_3$ . In the Appendix, these matrix elements are put into a form suitable for numerical computations.

The diagonalization of  $\hat{H}_3 + \hat{H}_4$  within the basis set gives rise to 12 Kramers doublets  $|\alpha=1\dots12,\ \pm\rangle$  which are certain linear combinations of the base vectors

$$|a, \pm\rangle = x_{a1} | {}^{6}A_{1}, \pm 5/2\rangle + x_{a2} | {}^{6}A_{1}, \mp 3/2\rangle + x_{a3} | {}^{4}A_{2}, \mp 3/2\rangle \pm x_{a4} | {}^{4}E_{\pm}, \mp 1/2\rangle \pm x_{a5} | {}^{4}E_{\mp}, \pm 3/2\rangle \pm x_{a6} | {}^{2}B_{2}, \pm 1/2\rangle + x_{a7} | {}^{2}E_{\mp}, \mp 1/2\rangle + x_{a8} | {}^{6}A_{1}, \pm 1/2\rangle + x_{a9} | {}^{4}A_{2}, \pm 1/2\rangle \pm x_{a10} | {}^{4}E_{\pm}, \pm 3/2\rangle \pm x_{a11} | {}^{4}E_{\mp}, \mp 1/2\rangle + x_{a12} | {}^{2}E_{\pm}, \mp 1/2\rangle .$$

$$(13)$$

The eigenvalues  $E_a$  and the eigenvectors  $x_{a\mu}$  of the Kramers doublets depend upon the six adjustable parameters  $\varepsilon_1$ ,  $\varepsilon_2$ ,  $\varepsilon_3$ ,  $\xi$ , D, and E. If we calculate in a final step the g-tensor and the paramagnetic susceptibility as a function of  $E_a$  and  $x_{a\mu}$ , then we can evidently fit the six parameters, at least in principle, to the corresponding experimental results.

The interaction with an external magnetic field  $\mathbf{H}$  may be treated as a perturbation; its corresponding Hamiltonian  $\hat{\mathbf{H}}_5$  is given by

$$\hat{\mathbf{H}}_{5} = \beta_{0} \, \boldsymbol{H} \, (\boldsymbol{L} + g_{0} \, \boldsymbol{S}), \tag{14}$$

where  $\beta_0 = 0.4669 \, (\mathrm{cm^{-1}/T})$  is the Bohr magneton (1 Tesla = 10 KG), and  $g_0 = 2.0023$  is the electronic g factor. It is straightforward to evaluate the relevant matrix elements of the operator  $\boldsymbol{J} = \boldsymbol{L} + g_0 \, \boldsymbol{S}$  within the Kramers doublets of Eqn (13). The contribution of the orbital angular momentum  $\boldsymbol{L}$  which depends implicitly upon  $\varepsilon_1$ ,  $\varepsilon_2$ , and  $\varepsilon_3$  is listed in the Appendix, though it becomes strongly quenched by the interactions  $\hat{\mathbf{H}}_1$  and  $\hat{\mathbf{H}}_4$ . On writing

$$\langle \alpha, \pm | \hat{J}_x | \beta, \pm \rangle = 0,$$
  
 $\langle \alpha, \pm | \hat{J}_x | \beta, \mp \rangle = C_{\alpha\beta}^x,$ 

$$\langle \alpha, \pm | \hat{\mathbf{J}}_{y} | \beta, \pm \rangle = 0,$$

$$\langle \alpha, \pm | \hat{\mathbf{J}}_{y} | \beta, \mp \rangle = \pm i C_{\alpha\beta}^{y},$$

$$\langle \alpha, \pm | \hat{\mathbf{J}}_{z} | \beta, \pm \rangle = \pm C_{\alpha\beta}^{z},$$

$$\langle \alpha, \pm | \hat{\mathbf{J}}_{z} | \beta, \mp \rangle = 0,$$
(15)

where the  $C^i_{\alpha\beta}$  are functions of  $x_{\alpha\mu}$  and  $x_{\beta\nu}$ , we obtain by perturbation theory up to second order the magnetic field dependent g-tensor components  $g^i_{\alpha}$  of the Kramers doublets  $|\alpha, \pm\rangle$ 

$$g_{\alpha}^{i} = 2 C_{\alpha\alpha}^{i} - 2 (\beta_{0} H^{i})^{2} \sum_{\beta \neq \alpha} \frac{(C_{\alpha\beta}^{i})^{2} (C_{\alpha\alpha}^{i} - C_{\beta\beta}^{i})}{(E_{\alpha} - E_{\beta})^{2}}.$$

$$(16)$$

The superscript i corresponds to x, y, z, respectively. The paramagnetic susceptibility can be derived in a similar way. With the aid of the abbreviations

$$\lambda_{\alpha\pm}^{i} = \sum_{\beta \pm \alpha} \frac{(C_{\alpha\beta}^{i})^{2}}{(E_{\alpha} - E_{\beta}) \pm \beta_{0} H^{i} (C_{\alpha\alpha}^{i} - C_{\beta\beta}^{i})}$$
 (17 a)

and

$$E_{\alpha\pm}^{i} = E_{\alpha} \pm \beta_{0} H^{i} C_{\alpha\alpha}^{i} + (\beta_{0} H^{i})^{2} \lambda_{\alpha\pm}^{i},$$
 (17b)

the susceptibility  $X^i$  becomes

$$X^{i}(T) = (N \beta_{0}/H^{i}) \sum_{\alpha} \left[ (C^{i}_{\alpha\alpha} - 2 \beta_{0} H^{i} \lambda^{i}_{\alpha-}) \exp(-E^{i}_{\alpha-}/kT) - (C^{i}_{\alpha\alpha} + 2 \beta_{0} H^{i} \lambda^{i}_{\alpha+}) \exp(-E^{i}_{\alpha+}/kT) \right] / \sum_{\alpha} \left[ \exp(-E^{i}_{\alpha-}/kT) + \exp(-E^{i}_{\alpha+}/kT) \right], \quad (18)$$

where N is Avogadro's number, and  $H^i$  is the ith component of the applied magnetic field. The magnetic susceptibility observed for a random sample is

$$\overline{X(T)} = 1/3(X^x + X^y + X^z).$$
 (19)

## III. Analysis of Experimental Data for Metmyoglobin, Metmyoglobin Fluoride, and Methemoglobin

The available frequency range for the far-infrared measurements of these compounds 11 was approxi-

mately 3.5-16 cm<sup>-1</sup>. The spectra show absorptions corresponding to the Zeeman splitting of the ground doublet  $\Delta E_1(H)$  in applied fields up to 52.2 kOe. According to Eqn (16), this splitting is given by

$$\Delta E_1^i = g_1^i \,\beta_0 \, H^i \,. \tag{20}$$

It should be noticed, however, than Eqn (16) was derived under the supposition that the Zeeman splittings are small compared with the relative energies of the Kramers doublets. Setting  $g_1^{\perp} \cong 6$ , we find the high-field limit of Eqn (20) to be ap-

proximately 15 kOe and 25 kOe for MbF and metMb, respectively. For that reason, the curves in Figs 4 and 5 were calculated by an exact treatment,

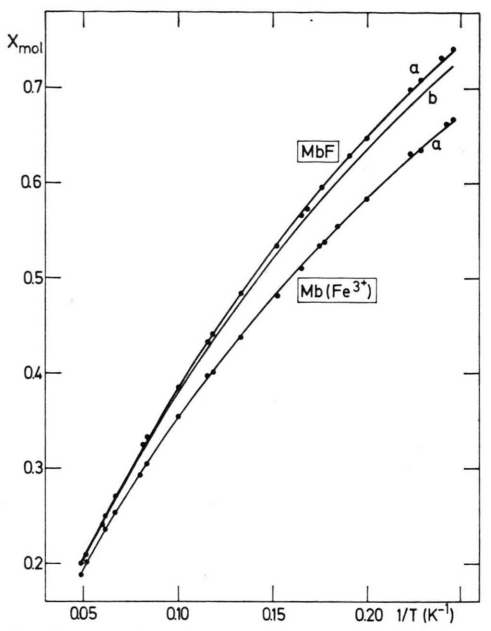


Fig. 3. Paramagnetic susceptibility of metMb and MbF as calculated from the corresponding fits in Tables III and IV. The experimental points were read from Fig. 1 of ref. <sup>10</sup>.

where the interaction  $\hat{H}_5$  is diagonalized together with  $\hat{H}_3 + \hat{H}_4$ . Absorption corresponding to a zero-field splitting  $E_2 - E_1 = 11.88 \pm 0.16 \; \mathrm{cm}^{-1}$  between the two lowest Kramers doublets was observed in the spectrum of MbF (in the remainder of the paper we set  $E_1 = 0$ ). However, no absorptions were found in zero field below the maximum frequency limit of  $\sim 16 \; \mathrm{cm}^{-1}$  for metMb and metHb. This observation implies  $E_2 \gtrsim 16 \; \mathrm{cm}^{-1}$  for these complexes; a more accurate estimate of  $E_2$  was deduced from the data for the Zeeman splitting of the ground doublet <sup>11</sup>, yielding  $E_2(\mathrm{metMb}) = 19.0 \pm 3.0 \; \mathrm{cm}^{-1}$  and  $E_2(\mathrm{metHb}) \cong 21 \; \mathrm{cm}^{-1}$ .

Magnetic susceptibility measurements on random samples of hemoproteins down to 4.2 K have been reported by Tasaki *et al.* <sup>10</sup>. The magnitude of the applied field was 12 kOe. The experimental data for metMb ( $p_{\rm H}=6$ ) and MbF are shown in Fig. 3 within the accuracy that  $X_{\rm exp}(T)$  can be read from Fig. 1 of ref. <sup>10</sup>. In order to compare the experimental data with the paramagnetic susceptibility X(T) as obtained from Eqns (18) and (19), we must introduce two further parameters n and  $X_{\rm dia}$ 

$$X_{\rm exp}(T) = n X(T) + X_{\rm dia}. \tag{21}$$

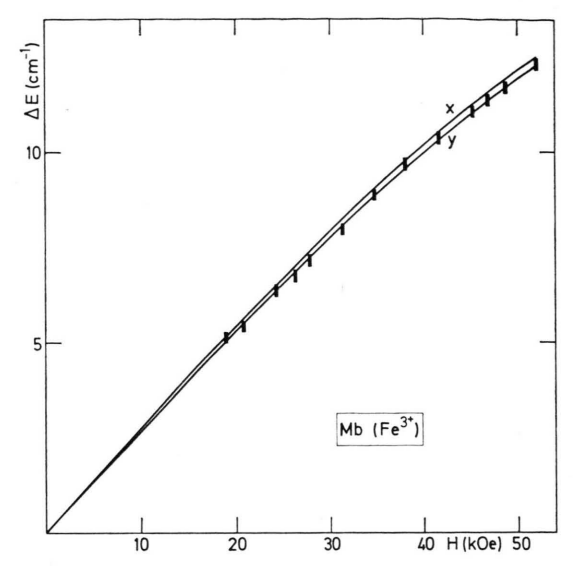


Fig. 4. Zeeman splitting of the ground doublet for metMb as calculated from fit a in Table III. The graphs x and y correspond to magnetic fields applied in the x and y direction, respectively. The bars are the measured absorption maxima read from Fig. 13 of ref. 11.

The diamagnetic part  $X_{\rm dia}$  is a trivial parameter which could be easily determined by the fit procedure, because it is not correlated with the adjustable parameters of the theory. The factor n corrects a possible experimental error by the determination of the number of iron ions in the samples; a conservative estimate is  $n = 1.00 \pm 0.02$ . The magnetic susceptibility of metHb is considerably smaller than that expected from a high-spin compound. During the course of repeated measurements 17, the value of the susceptibility was found to vary from time to time in the same sample preparation. It is assumed, therefore, that a fluctuating portion of the iron ions of metHb has a low-spin ground state, so that these measurements are unsuitable for our fit procedure.

The g-tensor is defined in the principal axes system (x, y, z) by the corresponding spherical polar angles  $(\vartheta, \varphi)$ 

$$g(\vartheta,\varphi) = \sqrt{(g_x^2 \cos^2 \varphi + g_y^2 \sin^2 \varphi) \sin^2 \vartheta + g_z^2 \cos^2 \vartheta}.$$
 (22)

The magnetic field dependent components  $g_x$ ,  $g_y$ ,  $g_z$  can be evaluated from Eqn (16). Kotani et al. <sup>12</sup> have measured the anisotropy of the g-tensor in the hem plane ( $\vartheta = \pi/2$ ) of single crystals of MbF and metMb. From these data (Figs 1 and 2 of ref. <sup>12</sup>), we determined by a least squares fit the principal

components  $g_x$ ,  $g_y$  and the angles  $\varphi$  which correspond to the maximum g-values  $(\vartheta = \pi/2)$  in the a b-plane and b  $c^*$ -plane, respectively, yielding

MbF: 
$$g_x(10 \, \text{GHz}) = 6.048 \pm 0.003,$$
  
 $g_y(10 \, \text{GHz}) = 5.870 \pm 0.005,$   
 $\varphi_{ab} = (20.7 \pm 1.2)^{\circ},$   
 $\varphi_{bc^*} = (-101.7 \pm 1.2)^{\circ},$   
metMb:  $g_x(10 \, \text{GHz}) = 5.979 \pm 0.004,$   
 $g_y(10 \, \text{GHz}) = 5.845 \pm 0.007,$   
 $\varphi_{ab} = (14.6 \pm 2.0)^{\circ},$   
 $\varphi_{bc^*} = (-107.8 \pm 2.0)^{\circ}.$ 

Additional measurements of the maximum g-values in the a b-plane  $g(\vartheta=\pi/2, \varphi_{ab})$  for single type A crystals of metMb and MbF at 34 and 55 GHz were reported by Gray et al. <sup>13</sup>. Less accurate measurements on metHb were also reported <sup>13</sup> for a single type A crystal in the a b- and b c\*-plane, and for the low-field extrema ( $\cong g_x$ ) of a polycrystalline sample. It is assumed in our analysis that the angles  $\varphi_{ab}$  and  $\varphi_{bc}$ \* for metHb are equal to those of metMb. The experimental data are listed in the Tables III - V.

We are now in the position to determine the six adjustable parameters  $\varepsilon_1$ ,  $\varepsilon_2$ ,  $\varepsilon_3$ ,  $\xi$ , D, and E of the theory. As outlined in Sec. II, the rhombic perturbation is already defined by a certain linear combination of D and E from those experiments discussed above. Fig. 2 shows the correlation between D and E for MbF, metMb, and ferrous Mb 9 obtained by the fit procedure. If the rhombic parameters are similar for ferric and ferrous hem compounds, the value of E can be placed in the vicinity of  $E \cong 250 \text{ cm}^{-1}$ . The small  $\pi$ -antibonding <sup>5, 8</sup> energy gap  $\varepsilon_1$  does not affect the fit procedure of ferric high-spin hem compounds within an allowed energy range of  $100\,\mathrm{cm^{-1}} < \varepsilon_1 < 800\,\mathrm{cm^{-1}}$ . It is probable true that  $\varepsilon_1$  is slightly larger than in ferrous Mb and HbA, where  $\varepsilon_1$  was found to be about 8  $100\,\mathrm{cm^{-1}}$ . The spin-orbit coupling constant  $\xi$  should have the same value in the various ferric hem complexes. In analogy to ferrous compounds 8 one expects a value of about 290 cm<sup>-1</sup>. A free fit to the experimental data of metMb and MbF places  $\xi$  in the range  $\xi = 300 \pm 25 \text{ cm}^{-1}$ . According to this dis-

	Fit a	Fit b	Experim. data
$\varepsilon_{2}$ (cm <sup>-1</sup> )	13941±37	13756±65	
$\varepsilon_3 (\text{cm}^{-1})$	$23595 \pm 38$	$23617 \pm 33$	
$D(\text{cm}^{-1})$	$-464 \pm 25$	$-496 \pm 29$	
$g_x(10 \text{ GHz})$	5.981	5.981	$5.979 \pm 0.004$ ref. <sup>12</sup>
$g_{y}(10 \text{ GHz})$	5.847	5.847	$5.845 \pm 0.007$ ref. <sup>12</sup>
$g_{ab}$ (34 GHz)	5.967	5.967	$5.971 \pm 0.004$ ref. <sup>13</sup>
$g_{ab}$ (55 GHz)	5.956	5.958	$5.958 \pm 0.005$ ref. <sup>13</sup>
$E_2  (\text{cm}^{-1})$	16.05	17.18	19.0 ± 3.0 ref. 11
$E_3  (\text{cm}^{-1})$	64.93	66.06	
$E(^{4}A_{2})$ (cm <sup>-1</sup> )	1406	1384	
$E(^{2}E_{+})$ (cm <sup>-1</sup> )	1225	1403	
$E(^{2}E_{-})$ (cm <sup>-1</sup> )	901	1025	
$E(^{2}B_{2})(cm^{-1})$	1636	1797	
$E(^{4}E)(cm^{-1})$	4943	4947	

Table III. Least squares results of the fitting procedure for the parameters  $\varepsilon_2$ ,  $\varepsilon_3$ , and D in metMb. The two fits a and b refer to  $n\!=\!1$  and  $n\!=\!1.02$  of Eqn (21), respectively.  $E_1\!=\!0$ ,  $E_2$ , and  $E_3$  are the relative energies of the three lowest Kramers doublets. The energies  $E(^4\!A_2)$ ,  $E(^2\!E_\pm)$ ,  $E(^2\!B_2)$ , and  $E(^4\!E)$  correspond to the base vectors of Eqn (8) in the absence of spin-orbit coupling.

	Fit a	Fit $b$	Fit c	Experim. data
$\begin{array}{c} \varepsilon_2(\mathrm{cm}^{-1}) \\ \varepsilon_3(\mathrm{cm}^{-1}) \\ D(\mathrm{cm}^{-1}) \\ D(\mathrm{cm}^{-1}) \\ g_x(10~\mathrm{GHz}) \\ g_{ab}(34~\mathrm{GHz}) \\ g_{ab}(55~\mathrm{GHz}) \\ E_2(\mathrm{cm}^{-1}) \\ E(^4A_2)(\mathrm{cm}^{-1}) \\ E(^2E_+)(\mathrm{cm}^{-1}) \\ E(^2E)(\mathrm{cm}^{-1}) \\ E(^2E)(\mathrm{cm}^{-1}) \end{array}$	$14572 \pm 128$ $22887 \pm 113$ $-639 \pm 129$ $6.050$ $5.873$ $6.015$ $5.990$ $10.83$ $40.18$ $2107$ $1482$ $870$ $1698$ $5470$	$14414\pm100$ $23016\pm85$ $-615\pm90$ $6.046$ $5.868$ $6.012$ $5.992$ $11.74$ $43.49$ $1979$ $1481$ $901$ $1729$ $5379$	$\begin{array}{c} 14440 \pm 135 \\ 22932 \pm 115 \\ -660 \pm 140 \\ 6.048 \\ 5.873 \\ 6.014 \\ 5.992 \\ 11.35 \\ 41.35 \\ 2062 \\ 1577 \\ 922 \\ 1784 \\ 5447 \end{array}$	$6.048\pm0.003$ ref. $^{12}$ $5.870\pm0.005$ ref. $^{12}$ $6.008\pm0.003$ ref. $^{13}$ $5.967\pm0.004$ ref. $^{13}$ $11.88\pm0.16$ ref. $^{11}$

Table IV. Least squares results of the fitting procedure for the parameters  $\varepsilon_2$ ,  $\varepsilon_3$ , and D in MbF. The fit criteria of the three fits are described in the text.  $E_1{=}0$ ,  $E_2$ , and  $E_3$  are the relative energies of the three lowest Kramers doublets. The energies  $E(^4A_2)$ ,  $E(^2E_{\pm})$ ,  $E(^2B_2)$ , and  $E(^4E)$  correspond to the base vectors of Eqn (8) in the absence of spin-orbit coupling.

	Fit	Experim. data (ref. 13)
$\begin{array}{l} \varepsilon_2(\text{cm}^{-1}) \\ \varepsilon_3(\text{cm}^{-1}) \\ D(\text{cm}^{-1}) \\ D(\text{cm}^{-1}) \\ g_x(34 \text{ GHz}) \\ g_x(55 \text{ GHz}) \\ g_{ab}(34 \text{ GHz}) \\ g_{ab}(55 \text{ GHz}) \\ g_{bc}*(34 \text{ GHz}) \\ E_2(\text{cm}^{-1}) \\ E_3(\text{cm}^{-1}) \\ E(^4A_2) (\text{cm}^{-1}) \\ E(^2E_+) (\text{cm}^{-1}) \\ E(^2E) (\text{cm}^{-1}) \\ E(^4E) (\text{cm}^{-1}) \end{array}$	$\begin{array}{c} 12455 \pm 2260 \\ 23890 \pm 174 \\ -528 \pm 59 \\ 5.961 \\ 5.956 \\ 5.950 \\ 5.946 \\ 5.810 \\ 23.87 \\ 83.20 \\ 1114 \\ 2370 \\ 1944 \\ 2810 \\ 4871 \end{array}$	5.990±0.025 polycrystalline 5.98 ±0.03 polycrystalline 5.938±0.005 single crystal 5.94 ±0.01 single crystal 5.80 ±0.03 single crystal ≈21 ref. <sup>11</sup>

Table V. Least squares results of the fitting procedure for the parameters  $\varepsilon_2$ ,  $\varepsilon_3$ , and D in metHb.  $E_1 = 0$ ,  $E_2$ , and  $E_3$  are the relative energies of the three lowest Kramers doublets. The energies  $E(^4A_2)$ ,  $E(^2E_{\pm})$ ,  $E(^2B_2)$ , and  $E(^4E)$  correspond to the base vectors of Eqn (8) in the absence of spin-orbit coupling.

cussion, we can reduce the least squares procedure to three of the six adjustable parameters, keeping  $\varepsilon_1$ ,  $\xi$ , and E constant at the nominal values

$$\varepsilon_1 = 200 \text{ cm}^{-1}, \quad \xi = 300 \text{ cm}^{-1}, \quad E = 250 \text{ cm}^{-1}. \quad (24)$$

Small deviations of  $\varepsilon_1$  and  $\xi$  from these values cause only a slight and systematic modification of the adjustable parameters  $\varepsilon_2$  and  $\varepsilon_3$  which does not affect our conclusions concerning the spatial arrangement of the ferric ion in these compounds, whereas E is only correlated to the rhombic fit parameter D.

The results of the least squares procedure are summarized in Tables III - V. In the case of metMb (Tab. III), the three parameters  $\varepsilon_2$ ,  $\varepsilon_3$ , and D were varied until the best fit with both the EPR and susceptibility data was obtained; no fit to the estimated value 11 of the zero-field splitting  $E_2$  was included in this procedure. The two fits a and b refer to n=1 and n=1.02 of Eqn (21), respectively. The theoretical susceptibilities of both fits correspond, within the accuracy of the drawing, to curve a in Fig. 3. Fig. 4 shows the Zeeman splittings of the ground doublet obtained from fit a, when the magnetic field is oriented along the x and y direction, respectively. The measured absorption maxima fit the lower  $\Delta E_1^y$  curve as expected from physical reasoning. The results for MbF are listed in Table IV. Fit a was performed in analogy to fit a of metMb, whereas the least squares criteria of fit b include the measured zero-field splitting  $E_2$  = 11.88 cm<sup>-1</sup>. In neither case is the agreement with both the far-infrared and susceptibility data (curves a, b of Fig. 3) perfect. It should be noticed, however, that the discrepancies between curve b and the experimental data can be removed by choosing a rather large n = 1.027 in Eqn (21). Finally, the results of a least squares procedure, including EPR and susceptibility data but no far-infrared data, are shown in fit c, when n was also handled as a fit parameter, yielding  $n = 1.015 \pm 0.004$ . Here, the calculated frequencies of the far-infrared absorptions are in accordance with the experimental data as shown in Fig. 5. The only discrepancy between theory and experiment was found for the  $g_{ab}$ -value at 55 GHz, which certainly arises from an error due to sample misorientation. The least squares fit criteria for metHb include only EPR data of limited accuracy (Table V) so that the error of the fit parameter  $\varepsilon_2$  is exceedingly large, though the calculated zero-field splitting is in reasonable agreement with the estimated value <sup>11</sup> of  $E_2 \cong 21 \text{ cm}^{-1}$ . This should be kept in mind in the subsequent discussion of the iron geometry relative to the hem plane and to the axial ligands at the 5th and 6th coordination.

In hemoproteins, the iron cation is approximately  $C_{4y}$ -coordinated to the four pyrrole nitrogens of the porphyrin ring and to the hem-linked nitrogen atom N<sub>s</sub> of histidine F8. The sixth coordination position of the ferric ion is occupied by a water molecule in metMb and metHb or a fluoride ion in MbF. The binding strengths of these ligands with the iron cation are closely related to the energy gaps  $\varepsilon_2 = E(3d_{z^2})$  $-E(3d_{xy})$  and  $\varepsilon_3 = E(3d_{x^2-y^2}) - E(3d_{xy})$  between the  $\sigma$ -antibonding  $3d_{z^2}$  and  $3d_{x^2-y^2}$  orbitals and the nonbonding  $3d_{xy}$  orbital. It was shown by means of group theoretical arguments 5 that the  $3d_{x^2-y^2}$  orbital interacts solely with the porphyrin  $\sigma$ -system, while the 3dz2 orbital reacts very sensitively upon the binding strengths of the axial ligands; tight binding of the iron cation with the axial ligands or

the porphyrin ring lifts up the energy  $\varepsilon_2$  or  $\varepsilon_3$ , respectively. The results of the fitting procedure in Tables III - V yield a decreasing binding strength  $\varepsilon_3$  of the ferric ion with the porphyrin ring in the sequence metHb-metMb-MbF which is obviously due to an increasing out of plane position of the iron cation, while its binding strength  $\varepsilon_2$  with the axial ligands shows a reversed behaviour. This is consistent with physical reasoning, because the iron geometry relative to the neighboring ligands is governed by the corresponding binding strengths: A lengthening of the distance between the iron and the pyrrole nitrogens in the hem plane is expected, if the binding strength with an axial ligand becomes more dominant. Thus, the more planar situation in metHb compared with metMb is likely caused by a larger displacement of the histidine F8 from the porphyrin ring. This reciprocal relationship between the out of plane position of the iron cation and its bond length with the N<sub>e</sub> nitrogen of the proximal histidine which is in contradiction 9, 18 with the Perutz model 19, was also found 8 for ferrous Mb and HbA. In the ferrous compounds, however, the more planar geometry was observed in Mb.

According to Eqn (8), the binding strength  $\varepsilon_3$ determines the energy of the 4A2 level which is responsible for the zero-field splitting of the lowest Kramers doublets in high-spin compounds via spin-orbet coupling. In planar high-spin compounds the low-lying  ${}^4\!A_2$  level gives rise to a large zero-field splitting. It is interesting to note that the zero-fied splitting for the fluoro derivatives of myoglobin, hemoglobin, and protoheme are very similar 11, indicating that the relative large out of plane position of the ferric ion is mainly determined by the strong bonding with the fluoride ion. Consequently, the ferric ion should be shifted towards the fluoride ion in these compounds. On the other hand, the fit data in Table V indicate that the near planar iron in metHb interacts only slightly with its axial ligands. Thus, it seems possible to me that metHb has an inversion motion in analogy to the ammonia molecule NH3, so that the ferric ion can vibrate through the center of the hem plane. This should be kept in mind by the analysis of the experimental susceptibility data of metHb which were found to be considerably smaller than those expected for high-spin compounds.

The approach of this paper can also be extended to low-spin compounds. In hemoproteins is the

binding strength of the four pyrrole nitrogens relatively weak, so that the  $^4A_2$  term lies at least  $\sim 1100~\rm cm^{-1}$  above the  $^6A_1$  term. Tight binding of the axial ligands with the iron cation lifts up the energy  $\varepsilon_2$ . In this case the rhombic split  $^2E$  term becomes the ground state which is characterized by a large anisotropy of the g-tensor.

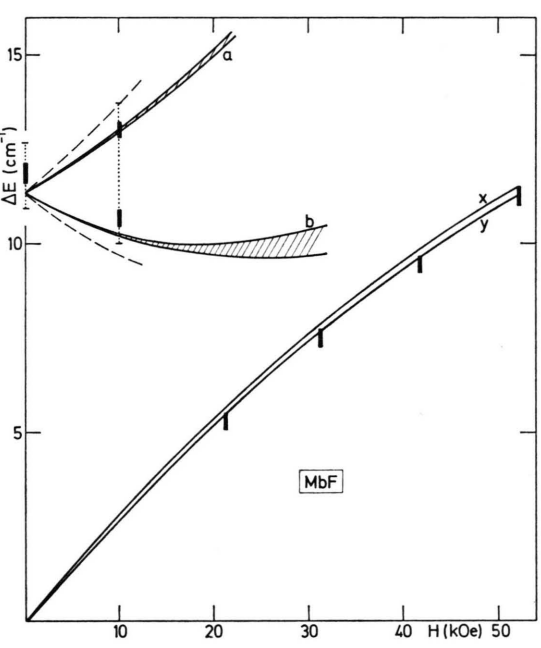


Fig. 5. Far-infrared transitions in MbF as calculated from fit c in Tab. IV. The graphs x and y correspond to the Zeeman splitting of the ground doublet  $\Delta E_1 = E_{1+} - E_{1-}$  in magnetic fields applied in the x and y direction, respectively. The shaded areas a and b cover the transition frequencies  $E_{2\pm} - E_{1-}$  and  $E_{2\pm} - E_{1+}$  for  $H \perp z$ , respectively. The dashed lines limit the region of additional weak absorption. The bars are the measured absorption maxima, and the dotted error flags indicate the approximate width of the observed absorptions as read from Fig. 12 of ref. <sup>11</sup>. It is expected that the absorption maxima fit the lower  $\Delta E_1 y$  curve and the strong transition area a, and are slightly shifted above the weaker transition area b, because the averaging over crystallite orientations contributes to this maximum.

#### Appendix

In this Appendix, the matrix elements of the operators  $\hat{H}_3$ ,  $\hat{H}_4$ ,  $\hat{L}_z$ , and  $\hat{L}_{\pm} = \hat{L}_x \pm i \hat{L}_y$  within the base vectors  ${}^6A_1$ ,  ${}^4A_2$ ,  ${}^4E$ ,  ${}^2B_2$ , and  ${}^2E$  are put into a form suitable for numerical computations. The empirical formulas were obtained by a linear least squares interpolation of exact matrix elements which were calculated for a variety of reasonable  $\varepsilon_1$ ,  $\varepsilon_2$ ,  $\varepsilon_3$  values defined in Eqn (7). Deviations from the exact matrix elements are less than 2%,

Table A1. The coefficients  $a_{\mu\nu}$  defined in Eqn (A1).

μ	$a_{\mu0}$	$a_{\mu 1} \cdot 10^6$	$a_{\mu 2} \cdot 10^{6}$	$a_{\mu 3} \cdot 10^{6}$
1	-0.620	0	0	-0.7
2	-0.632	0	-14	14
3	-0.644	11	24	-31
4	2.154	-22	12	0
5	-0.264	11	51	-58
6	1.935	-6	93	-92
7	2.608	-7	19	-10
8	-1.503	-6	5	-2
9	1.279	-11	14	-6
10	-0.271	2	-58	56
11	1.879	-4	45	-41
12	-0.728	6	-8	0
13	-0.797	6	-8	0
14	0.134	118	-67	63
15	1.175	-6	16	-11
16	-1.302	-11	17	-14
17	-2.295	-9	25	-1

if the corresponding base vectors lie at most  $4000 \, \mathrm{cm^{-1}}$  above the particular ground state. With the aid of the interpolation formula

$$M_{\mu} = a_{\mu 0} + a_{\mu 1} \cdot \varepsilon_1 + a_{\mu 2} \cdot \varepsilon_2 + a_{\mu 3} \cdot \varepsilon_3, \qquad (A1)$$

where the  $a_{\mu\nu}$  are listed in Table A1, we obtain the following nonvanishing matrix elements:

$$\begin{split} & \langle {}^{4}\mathbf{A}_{2} - 3/2 \mid \hat{\mathbf{H}}_{3} \mid {}^{6}\mathbf{A}_{1} - 3/2 \rangle = -\, \xi\,(2)^{\,\text{1/2}}\,M_{1} \\ & \langle {}^{4}\mathbf{A}_{2} - 1/2 \mid \hat{\mathbf{H}}_{3} \mid {}^{6}\mathbf{A}_{1} - 1/2 \rangle = -\, \xi\,(3)^{\,\text{1/2}}\,M_{1} \\ & \langle {}^{4}\mathbf{E}_{-} - 3/2 \mid \hat{\mathbf{H}}_{3} \mid {}^{6}\mathbf{A}_{1} - 5/2 \rangle = -\, \xi\,(5)^{\,\text{1/2}}\,M_{2} \\ & \langle {}^{4}\mathbf{E}_{+} - 1/2 \mid \hat{\mathbf{H}}_{3} \mid {}^{6}\mathbf{A}_{1} - 3/2 \rangle = -\, \xi\,(3)^{\,\text{1/2}}\,M_{2} \\ & \langle {}^{4}\mathbf{E}_{-} - 1/2 \mid \hat{\mathbf{H}}_{3} \mid {}^{6}\mathbf{A}_{1} - 1/2 \rangle = -\, \xi\,(3/2)^{\,\text{1/2}}\,M_{2} \end{split}$$

- G. M. Harris and M. Weissbluth, Phys. Rev. 149, 198-200 [1966].
- <sup>2</sup> G. Harris, J. Chem. Phys. 48, 2191-2214 [1968].
- <sup>3</sup> R. L. Ake and G. M. Harris Loew, J. Chem. Phys. 52, 1098-1114 [1970].
- <sup>4</sup> G. M. Harris Loew, Biophys. J. 10, 196-212 [1970].
- <sup>5</sup> H. Eicher and A. Trautwein, J. Chem. Phys. **50**, 2540—2551 [1969]; **52**, 932—934 [1970].
- <sup>6</sup> H. Eicher, F. Parak, D. Bade, and J. Tejada, J. Phys. (Paris), C 6, 363-366 [1974].
- <sup>7</sup> B. H. Huynh, G. C. Papaefthymiou, C. S. Yen, J. L. Groves, and C. S. Wu, J. Chem. Phys. **61**, 3750-3758 [1974].
- 8 H. Eicher, D. Bade, and F. Parak, J. Chem. Phys. (received Nov. 4, 1974).
- <sup>9</sup> H. Eicher, to be published in Z. Naturforsch. c.
- <sup>10</sup> A. Tasaki, J. Otsuka, and M. Kotani, Biochim. Biophys. Acta **140**, 284-290 [1967].
- <sup>11</sup> G. C. Brackett, P. L. Richards, and W. S. Caughey, J. Chem. Phys. **54**, 4383-4401 [1971].

$$\begin{array}{llll} \langle^{4}{\rm E}_{+} & 3/2 \mid \hat{\rm H}_{3} \mid ^{6}{\rm A}_{1} & 1/2 \rangle = -\xi \, (1/2)^{\frac{1}{2}} \, M_{2} \\ \langle^{4}{\rm E}_{+} & -1/2 \mid \hat{\rm H}_{3} \mid ^{4}{\rm A}_{2} & -3/2 \rangle = & \xi \, (1/10)^{\frac{1}{2}} \, M_{3} \\ \langle^{4}{\rm E}_{+} & 3/2 \mid \hat{\rm H}_{3} \mid ^{4}{\rm A}_{2} & 1/2 \rangle = & \xi \, (1/10)^{\frac{1}{2}} \, M_{3} \\ \langle^{4}{\rm E}_{-} & -1/2 \mid \hat{\rm H}_{3} \mid ^{4}{\rm A}_{2} & 1/2 \rangle = -\xi \, (2/15)^{\frac{1}{2}} \, M_{3} \\ \langle^{2}{\rm E}_{-} & -1/2 \mid \hat{\rm H}_{3} \mid ^{4}{\rm A}_{2} & 1/2 \rangle = -\xi \, (1/12)^{\frac{1}{2}} \, M_{3} \\ \langle^{2}{\rm E}_{+} & -1/2 \mid \hat{\rm H}_{3} \mid ^{4}{\rm A}_{2} & 1/2 \rangle = -\xi \, (1/12)^{\frac{1}{2}} \, M_{4} \\ \langle^{4}{\rm E}_{\pm} & 3/2 \mid \hat{\rm H}_{3} \mid ^{4}{\rm E}_{\pm} & 3/2 \rangle = \pm \xi \, (3/20)^{\frac{1}{2}} \, M_{5} \\ \langle^{4}{\rm E}_{\pm} & -1/2 \mid \hat{\rm H}_{3} \mid ^{4}{\rm E}_{\pm} - 1/2 \rangle = \mp \xi \, (1/60)^{\frac{1}{2}} \, M_{5} \\ \langle^{2}{\rm E}_{\pm} & -1/2 \mid \hat{\rm H}_{3} \mid ^{4}{\rm E}_{\pm} - 1/2 \rangle = \pm \xi \, (1/6)^{\frac{1}{2}} \, M_{7} \\ \langle^{2}{\rm E}_{2} & 1/2 \mid \hat{\rm H}_{3} \mid ^{4}{\rm E}_{-} & -1/2 \rangle = -\xi \, 0.5 \, M_{7} \\ \langle^{2}{\rm E}_{2} & 1/2 \mid \hat{\rm H}_{3} \mid ^{2}{\rm E}_{2} & 1/2 \rangle = \pm \xi \, (1/6)^{\frac{1}{2}} \, M_{8} \\ \langle^{2}{\rm E}_{\pm} & -1/2 \mid \hat{\rm H}_{3} \mid ^{2}{\rm E}_{\pm} - 1/2 \rangle = \pm \xi \, (1/6)^{\frac{1}{2}} \, M_{9} \\ \langle^{2}{\rm E}_{-} & -1/2 \mid \hat{\rm H}_{3} \mid ^{2}{\rm E}_{\pm} - 1/2 \rangle = \pm \xi \, (1/6)^{\frac{1}{2}} \, M_{9} \\ \langle^{4}{\rm E}_{-} & -1/2 \mid \hat{\rm H}_{3} \mid ^{2}{\rm E}_{\pm} - 1/2 \rangle = D \cdot M_{10} + E \cdot M_{11} \\ \langle^{4}{\rm E}_{+} & 3/2 \mid \hat{\rm H}_{4} \mid ^{4}{\rm E}_{-} - 1/2 \rangle = D \cdot M_{10} + E \cdot M_{11} \\ \langle^{4}{\rm E}_{+} & 3/2 \mid \hat{\rm H}_{4} \mid ^{2}{\rm E}_{-} - 1/2 \rangle = D \cdot M_{12} + E \cdot M_{13} \\ \langle^{4}{\rm E}_{\pm} \mid \hat{\rm L}_{z} \mid ^{4}{\rm E}_{\pm} \rangle = \pm M_{14} \\ \langle^{2}{\rm E}_{\pm} \mid \hat{\rm L}_{z} \mid ^{4}{\rm E}_{\pm} \rangle = \pm M_{16} \\ \langle^{4}{\rm A}_{2} \mid \hat{\rm L}_{\pm} \mid ^{4}{\rm E}_{\mp} \rangle = \pm M_{16} \\ \langle^{4}{\rm A}_{2} \mid \hat{\rm L}_{\pm} \mid ^{2}{\rm E}_{\pm} \rangle = \pm M_{17} \\ \langle^{2}{\rm B}_{2} \mid \hat{\rm L}_{\pm} \mid ^{2}{\rm E}_{\pm} \rangle = \pm M_{17} \\ \langle^{2}{\rm B}_{2} \mid \hat{\rm L}_{\pm} \mid ^{2}{\rm E}_{\pm} \rangle = \pm M_{17} \\ \langle^{2}{\rm B}_{2} \mid \hat{\rm L}_{\pm} \mid ^{2}{\rm E}_{\pm} \rangle = \pm M_{17} \\ \langle^{2}{\rm B}_{2} \mid \hat{\rm L}_{\pm} \mid ^{2}{\rm E}_{\pm} \rangle = \pm M_{17} \\ \langle^{2}{\rm B}_{2} \mid \hat{\rm L}_{\pm} \mid ^{2}{\rm E}_{\pm} \rangle = \pm M_{17} \\ \langle^{2}{\rm B}_{2} \mid \hat{\rm L}_{\pm} \mid ^{2}{\rm E}_{\pm} \rangle = \pm$$

- <sup>12</sup> M. Kotani and H. Morimoto, Magnetic Resonance in Biological Systems, Pergamon Press, New York 1967.
- <sup>13</sup> A. L. Gray and H. A. Buckmaster, Can. J. Biochem. 51, 1142-1153 [1973].
- <sup>14</sup> G. Racah, Phys. Rev. **63**, 367-382 [1943].
- <sup>15</sup> B. R. Judd, Operator Techniques in Atomic Spectroscopy, Advanced Physics Monograph Series (W. A. Nierenberg, ed.), MacGraw-Hill Book, New York 1963.
- renberg, ed.), MacGraw-Hill Book, New York 1963.

  16 U. Gonser, Y. Maeda, A. Trautwein, F. Parak, and H. Formanek, Z. Naturforsch. 29 b, 241-244 [1974].
- <sup>7</sup> A. Tasaki, Probes of Structure and Function of Macro-molecules and Membranes, Vol. II, pp. 247-261, Academic Press, Inc., New York and London 1971.
- <sup>18</sup> H. Eicher, Proceedings of the International Conference on Mössbauer Spectroscopy 1975, Cracow (Poland), Vol. I.
- <sup>19</sup> M. F. Perutz, Nature **228**, 726-734 [1970]; **237**, 495-499 [1972].